Energy 263 (2023) 125909

Contents lists available at ScienceDirect

Energy

journal homepage: www.elsevier.com/locate/energy

Microwave calorimeter for dielectric and thermal analysis of materials

Juan R. Sánchez [a,b,*], José D. Gutiérrez-Cano [a], Pedro J. Plaza-González [a], Felipe L. Penaranda-Foix [a], José M. Catalá-Civera [a]

[a] ITACA Institute, Universitat Politècnica de València, Camino de Vera, 46022, Valencia, Spain
[b] GEM, Universidad Politécnica de Cartagena, Calle Ángel 32, 30202, Cartagena, Spain

ARTICLE INFO

Keywords:
Thermal analysis
Dielectric properties
Thermal properties
Microwave heating
Calorimetry

ABSTRACT

A fast method for microwave processing and measurement of dielectric and thermal properties of materials as a function of temperature has been developed (MW-DETA). Unlike previous approaches, the method provides totally new quantitative measurements of the thermal parameters, which are fundamental for calculating the specific heat and in particular, the energy requirements of electrification of materials processing via microwave heating.

The in-situ measurement of dielectric properties of the sample with temperature, together with the precise numerical modelling of the thermal process, provided the necessary information to quantify the thermal and microwave losses and, therefore, the precise amount of power delivered to the sample that is converted into heat.

Compared to conventional calorimeters, microwave heating reduces the experimental time and improves the uniformity of heating, which leads to a fast and reliable method to determine the thermal properties of the material under test with different operation modes, either constant or variable heating rates.

The functionality of the thermal parameters measurement system has been demonstrated by heating and measuring a ceramic sample of Macor up to 400 °C. Accuracy reached in the thermal process has been validated by comparison with a conventional DSC analysis.

1. Introduction

The measurement of the physical or chemical properties of materials and their transformations as a function of temperature is a principal goal from basic to many research and applied fields. During last years, the increasing demand of energy has brought the advent of new materials with advanced properties, including the materials that generate, store and transport energy, along with new processing techniques (microwaves, solar energy, etc.). This type of materials requires the development of new testing instruments and measurement methods capable to highlight their unique properties as well as their potential to store energy [1,2].

Thermal analysis (TA) refers to a series of techniques to characterize the physical and chemical properties of materials as a function of temperature and time [3–5]. The most common TA techniques are the Thermo- Gravimetric Analysis (TGA) [6], based on changes in mass, and the Differential Thermal Analysis (DTA) and the Differential Scanning Calorimetry (DSC) [7,8], based on temperature variations in the materials and their reactions to those changes. DTA and DSC are methods that measure enthalpy changes in a material when it is heated or cooled under certain conditions. Both methods allow the characterization of thermal properties as: specific heat c_p and thermal conductivity k [9].

The energy requirements to heat materials are associated with enthalpy or heat capacity changes, since every physical or chemical phenomenon involves an energy fluctuation. In particular, DSC is widely used for thermal analysis due to the simplicity to detect the heat transitions of materials. This type of equipment maintains the same temperature difference between the sample and an inert reference, measuring the needed supplied energy to each material. Nowadays DSC plays an important role in the characterization of a wide range of materials as polymers [10], electronic circuits [11], geological materials [12,13], etc.

DSC has proven to be a very reliable technique, but it still shows some limitations with the available equipment, as the extensive calibration procedures, the relatively large time-constant of the measurement system and the small sample size required in the fixtures [14].

* Corresponding author. ITACA Institute, Universitat Politècnica de València, Camino de Vera, 46022, Valencia, Spain.
E-mail addresses: juasncm1@upv.es (J.R. Sánchez), jdgutierrez@itaca.upv.es (J.D. Gutiérrez-Cano), pedplago@itaca.upv.es (P.J. Plaza-González), fpenaran@dcom.upv.es (F.L. Penaranda-Foix), jmcatala@dcom.upv.es (J.M. Catalá-Civera).

https://doi.org/10.1016/j.energy.2022.125909
Received 22 July 2022; Received in revised form 13 October 2022; Accepted 25 October 2022
Available online 5 November 2022

Abbreviations

0DM	Zero-Dimensional Model
CPM	Cavity Perturbation Method
DSC	Differential Scanning Calorimetry
DTA	Differential Thermal Analysis
FDSC	Fast Differential Scanning Calorimetry
FDTD	Finite Difference in Time Domain
MW-DETA	Microwave Differential and Thermal Analysis
MWTA	Microwave Thermal Analysis
TA	Thermal Analysis
TE	Transverse Electric
TGA	Thermogravimetric Analysis
TM	Transverse Magnetic
VNA	Vector Network Analizer

Different approaches for increasing the heating rate have been developed recently [15,16]. Fast DSC (FDSC) allows increasing the scanning rate several orders of magnitude, especially when cooling, micro- or nano-sized samples. However, this approach still needs improvements because very fast scanning results in poor resolution of close reactions and the small sample size makes difficult to weight the sample.

Microwave Thermal Analysis (MWTA) is also a recent technique for instruments that use microwaves to both heat and detect thermally induced transformations in materials [17,18]. The penetration of microwaves in the material reduces its temperature gradients with respect to conventional techniques, mostly based on conduction heating, thus, larger samples can be analyzed obtaining a better resolution of the thermal processes. This method presents the additional advantage of studying the direct interaction of microwaves with materials. This is of particular interest since microwaves are growing as a heating technology in industrial and research fields due to the reported evidence that they can enhance reaction rates and thermal transformations in materials and it is not fully understood if the attained rate enhancements are due to purely thermal effects, or non-thermal microwave effects [19–22].

For example, in Refs. [23,24] a MWTA instrument was developed in a rectangular waveguide to perform microwave differential thermal analysis with different working modes: constant power, linear power and linear heating. It combines the microwave heating with the differential temperature measurement to determine the thermal properties of materials. Susceptible cells containing small samples made difficult to distinguish between direct applied microwave heating and heat conduction from the cell.

Nesbitt et al. proposed in Ref. [25] a single mode resonant cavity for thermal analysis and dielectric measurements. TA was performed by measuring the different adjustments of the microwave power source required for heating a sample (sometimes respect to an inert reference sample). Microwave and thermal heat losses in the cavity were not evaluated, then measurements were restricted to relative differences when an either endothermic or exothermic reaction occurred.

In this paper, we describe a fast and accurate method for determining the dielectric and thermal properties of materials as a function of the temperature by microwave heating. The method, called MW-DETA (Microwave Dielectric and Thermal Analysis) is based on the cylindrical microwave reactor reported in Ref. [26] with new procedures to provide totally new quantitative measurements of the thermal parameters, improving the performance of previous reported microwave calorimeters with only differential results.

The temperature dependent dielectric properties measured by the equipment of [26] and the development of a numerical thermal model in the cavity has allowed the evaluation of the microwave and thermal losses in the cavity, which is fundamental to quantify the microwave power that contributes to the temperature increase in the materials.

In a similar manner to previous approaches, the MW-DETA can operate with different heating modes: constant microwave power, linear power, linear heating rate, etc. Experimental results of thermal properties of ceramic samples have been measured for temperatures varying from room temperature to 400 °C. The accuracy of the microwave TA has also been evaluated by comparing the results with conventional DSC techniques.

2. Design of the microwave calorimeter

Fig. 1a shows the schematic view of the microwave calorimeter designed for high-temperature dielectric and thermal property measurements (MW-DETA). The microwave calorimeter consists of a dual-mode cylindrical cavity where one electromagnetic mode is designed to heat a sample of material with high-power microwaves and the other mode is used to simultaneously measure dielectric properties as a function of the temperature [22].

The heating mode (TE_{111}), designed to resonate near 2.45 GHz, is fed into the cavity by a probe inserted through the side wall, while the measuring mode (TM_{010}) at 2.1 GHz, is fed by another probe through the bottom wall of the cavity. The E-field vector of the heating mode is perpendicular to the cavity axis and the E-field vector of the measuring mode is parallel to the cavity axis, both with maximum field magnitude at the center (see Fig. 1b). The sample of material (diameter 10 mm and height 15 mm) is placed in a quartz vial holder which is inserted into the cavity through a cutoff hole in the top wall. This sample size in the cylindrical tube is positioned at the maximum of E-field in the cavity to ensure uniform processing and testing.

The microwave heating source is a narrowband solid-state amplifier driven by the RF output of a Vector Network Analyzer (VNA) with a maximum power of 150 W. A power isolator placed after the amplifier protects against power reflected from the cavity. The output of the microwave amplifier launches the microwaves into the cavity via a directional coupler and a high-power coaxial cable. The directional coupler decouples the reflected signal from the cavity to the second channel of the network analyzer, monitoring the microwave power delivered to the cavity.

The measurement mode operates with a second VNA through a cross-coupling filter with more than 100 dB attenuation to avoid interferences between heating and measuring signals. Dielectric properties of materials as a function of temperature are calculated during heating by the cavity perturbation method (CPM) [26].

The cavity also incorporates two holes in the side wall for sample inspection with a video camera and for temperature measurement. The dimensions of all the open accesses to the cavity are designed to avoid any leakage of microwave energy outside the cavity.

The accurate determination of bulk temperature during microwave heating is a non-trivial topic and different approaches have been proposed for non-contact measurements, including thermochromic [27] or temperature-sensitive fluorescent [28], metal organic particles that change their colour or fluorescence, respectively, as a function of the in-situ temperature. In this work, the pyrometer (Optris CT-Laser LT) with an accuracy of 0.1 °C is used to determine the bulk temperature of the sample by measuring the surface temperature of the quartz reactor from outside of one of the microwave cavity access holes. A calibration is therefore needed to determine the correspondence between the measured temperature (quartz surface) and the sample bulk temperature. The implemented calibration procedure to determine this relationship is reported in Ref. [29].

Once tube and sample are positioned inside the cavity, a control software allows setting the desired heating rate, monitoring the sample temperature, recording the video image of the sample and the response of the cavity for both heating and measuring modes. The continuous measurement of the resonance parameters of the cavity (resonant frequency and quality factor) and the microwave power delivered to the

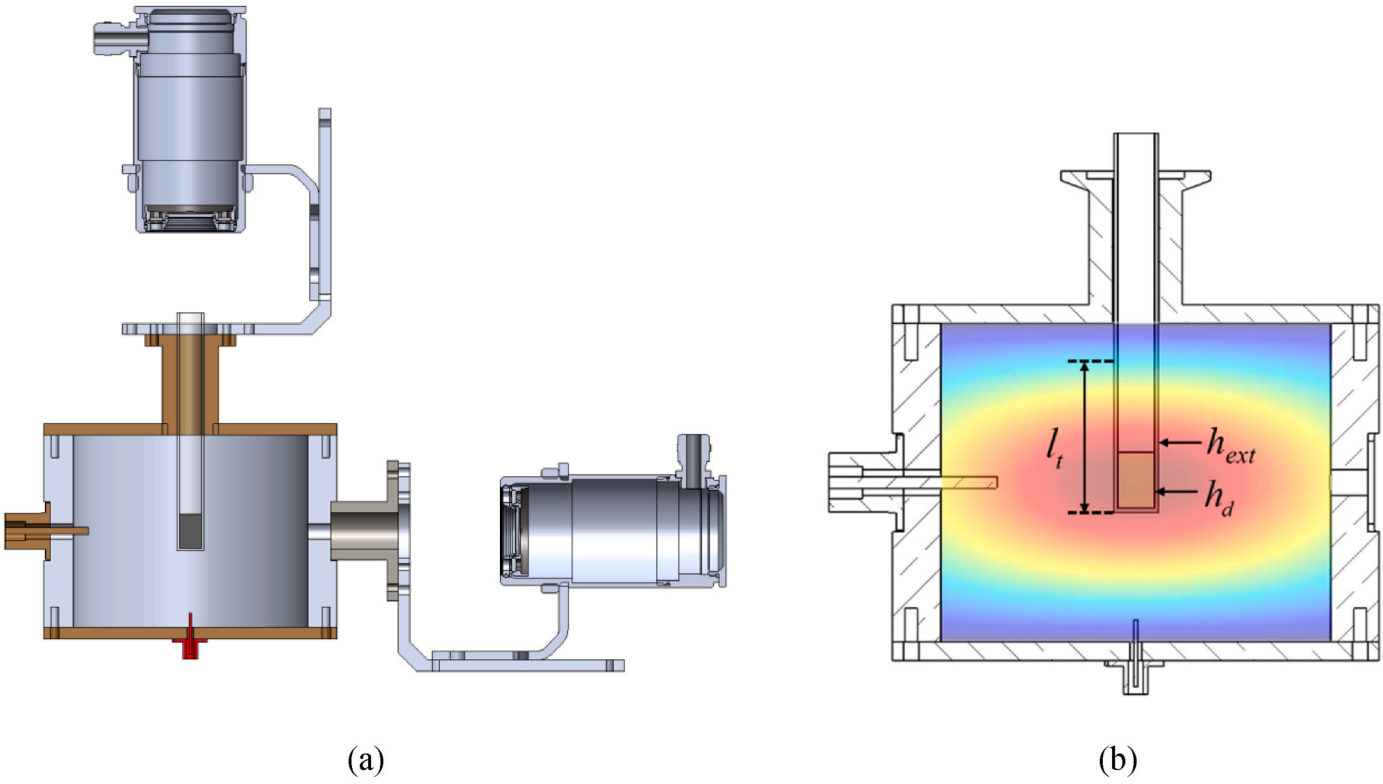

Fig. 1. (a) Schematic view of the microwave calorimeter (MW-DETA), (b) E-field distribution of the heating mode (TE_{111}) in the dual-mode microwave cavity.

cavity provides all the information for calculating the dielectric and thermal properties of the sample as a function of temperature.

3. Modelling of the microwave calorimeter

3.1. Microwave heating thermal model

Microwave heating of a dielectric material inside a microwave cavity is a process that involves electromagnetic waves and heat transfer. The conversion of microwave energy into heat depends on the dielectric properties of the materials and the frequency of the excitation [30]. The average microwave power P_d (W) absorbed by a sample of volume V (m^3) is given by the equation:

$$P_d = 2\pi f \varepsilon_o \varepsilon'' |E|^2 V \tag{1}$$

where ε'' is the dielectric loss factor of the material, f is the frequency of the excitation (Hz), and E is the microwave electric field strength (V/m).

From the first law of thermodynamics, the increase in heat quantity should equal the net inflow of heat and the net production of heat within this volume (subtracting the losses). Starting from this continuity relation, the temperature T in a material can be determined from the Fourier energy balance equation,

$$\rho c_P \frac{dT}{dt} = \nabla \cdot (k_T \cdot \nabla T) + \frac{1}{V}(P_d - P_{heat}) \tag{2}$$

where ρ is the density of the material (g/m^3), c_p is the specific heat (J/g°C), $\frac{dT}{dt}$ is the heating rate (°C/s), k_T is the thermal conductivity, and P_{heat} (W) refers to any contribution to the thermal losses in the sample.

Total losses in the cavity encompass the heat transfer of the material P_{heat} and also the microwave power absorbed by the metallic walls P_{walls}

$$P_{losses} = P_{walls} + P_{heat} = P_{walls} + P_{cond} + P_{conv} + P_{rad} \tag{3}$$

The heat transfer occurs by three basic mechanisms: conduction, convection, and radiation.

In conduction, heat is transferred from the hot to the cool area of a material. The rate at which heat is conducted within a sample is a function of the temperature difference in the sample and its ability to conduct heat, i.e. the thermal conductivity. In homogeneous and isotropic heat conductor materials with dimensions sufficiently small compared to the wavelength at the frequency of excitation, temperature gradients due to microwave heating can be assumed to be small and consequently, the conduction losses are minor [31,32]. These small temperature gradients suggest the use of a zero-dimensional model (0DM) where the bulk temperature of the material is evaluated as an average temperature of all material's volume to be a function of time only.

Convection describes the heat flow from the material surface and the tube container to the surrounding fluid or gas. If the motion of the fluid is not forced, the process is called natural convection and it is defined by the Newton's law of cooling, as follows [33]:

$$P_{conv} = h_c A (T - T_0) \tag{4}$$

where h_c is the heat transfer coefficient ($W/m^{2\circ}C$), A is the surface area of the body in contact with the fluid (m^2), T is the temperature of the material (°C), and T_0 is the temperature of the fluid surrounding the material surface (°C).

Radiation considers the emission of energy in the form of electromagnetic waves because of the high temperature in a material. Stefan-Boltzmann law describes the heat lost by radiation as follows:

$$P_{rad} = e\sigma A\left(T^4 - T_0^4\right) \tag{5}$$

where e is the material emissivity, σ is the Stefan-Boltzmann constant (W/m^2K^4) and A is the surface area, as defined in (4).

In certain environments, the radiation heat losses P_{rad} have also shown proportional to $(T - T_0)$ by defining a radiation heat transfer coefficient h_r [34] similar to the heat transfer coefficient of (4). Thus, the temperature evolution in a material is influenced by the combined effect of these two types of heat transfer. They are given in the interface

between the sample and the tube, and between the tube and the air, being not possible to entirely isolate one type of interaction from the other. When both convection and radiation are involved in the heat transfer, for simplicity, the heat losses can be evaluated by a model combining the Newton and the Stefan-Boltzmann laws for cooling. Then, the total power heat transfer is obtained by the linear superposition of the heat coefficients [35]:

$$P_{heat} = (h_c + h_r)A(T - T_0) = h_t A(T - T_0) \tag{6}$$

where h_t is an effective heat transfer coefficient for combined convective and radiative losses.

Therefore, assuming an average temperature in the homogeneous sample, the heating rate for the 0DM of Eq. (2) is given by the differential equation:

$$\frac{dT}{dt} = \frac{P_d}{mc_P} - \frac{h_t A}{mc_P}(T - T_0) = \frac{P_d}{C} - \frac{h_t A}{C}(T - T_0) \tag{7}$$

where m is the mass of the sample (g) and $C = mc_p$ is the heat capacity (J/°C). The heat capacity C refers to the material or materials into the cavity that experiment heating with the application of microwaves. In the case of the microwave calorimeter designed in Section 2, the sample of material is located inside a tube container, thus, the heat capacity of Eq. (7) refers to the heat capacity of a composed material. Here, an arithmetic weight fraction average of the component values is applied according to Ref. [36]:

$$C = m_d c_{P_d} + m_t c_{P_t} \tag{8}$$

where m_i, c_{Pi} are respectively, the mass and the specific heat of each component (sample and tube).

Then, the overall heat transfer coefficient h_t of Eq. (7) depends on the heat transfer of the tube (with the surrounding air in the cavity), quantified by an external heat transfer coefficient h_{ext} and also on the thermal resistance between the sample and the tube, also defined by a heat transfer coefficient h_d, although the boundary between the tube and the sample does not describe exactly a convective boundary condition [37,38]. This heat transfer coefficient h_d determines the thermal insulation of the sample in the tube as well as its temperature difference during microwave heating.

Both heat transfer coefficients can be combined as indicated in (9) [39] and they usually depend on temperature.

$$\frac{1}{h_t A} = \frac{1}{h_d A_d} + \frac{1}{h_{ext} A_{ext}} \tag{9}$$

where A_d refers to the surface of heat transfer between sample and tube and depends on the geometry of the sample, and A_{ext} refers to the area of the tube where convection and radiation occur in the cavity and depends on the heat exchange with the surrounding air.

The net power absorbed by the sample that contributes to the temperature increase is then determined as the difference of the microwave power applied to the sample and the heat losses.

$$P_{net} = P_d - h_t A(T - T_0) \tag{10}$$

From Eqs. (7) and (10), the combined heat capacity C of tube and sample can be obtained as the coefficient of the net power and the heating rate dT/dt as a function of the temperature:

$$C = \frac{P_{net}}{dT/dt} \tag{11}$$

and then, the specific heat of the material determined from (8).

The time evolution of the temperature in the material can be calculated by discretization of the heat Eq. (7), assuming a uniform distribution of temperature in the sample. Considering that the differential of the independent variable dt is equal to its increment Δt, if this time increment is small enough, the differential of temperature can be approximated as the increment of temperature.

$$dT \cong \Delta T = T_i - T_{i-1}, dt = \Delta t \tag{12}$$

Since both C and h_t experiment variations with temperature, the increase of the average temperature in a material exposed to microwaves could be calculated as a function of time as:

$$\frac{dT}{dt} \cong \frac{T_i - T_{i-1}}{\Delta t} = \frac{P_d}{C} - \frac{h_t A}{C}(T_{i-1} - T_0) \tag{13}$$

$$T_i = \frac{\frac{P_d \Delta t}{C_{i-1}} + \frac{(h_t A)_{i-1}}{C_{i-1}} T_0 \Delta t + T_{i-1}}{1 + \frac{(h_t A)_{i-1}}{C_{i-1}} \Delta t} \tag{14}$$

where the temperature T_i in each i-th time interval is calculated using the heat capacity C and the total heat transfer coefficient ($h_t A$) from the previous time step i-1.

We recall that we assumed a temperature distribution in the solid sufficiently uniform and a thermal conductivity high enough to neglect any gradient inside the sample, and then the temperature of the solid can be considered only function of time, the applied microwave power, and the thermal losses [32].

3.2. Electromagnetic-thermal simulations

To analyze the range of functionality of the zero-dimensional microwave thermal model (0DM) described by Eqs. 1–14, the microwave calorimeter described in previous section has been simulated with the aid of the electromagnetic software QuickWave (QW-3D).

QW-3D is a commercial three-dimensional electromagnetic simulation package based on the conformal FDTD method that includes a Basic Heat Module (BHM) offering the possibility to simulate the temperature evolution of objects under microwave heating [40].

After defining the specific geometry of Fig. 1a in the graphical editor (see Fig. 2a), including the (EM and thermal) boundary conditions in the material and tube, the QW-3D simulation process requires 3 steps. A first run in a broad range of frequencies to identify the resonant peak of the microwave cavity. A second run with a sinusoidal excitation at this frequency to calculate the E-field distribution in the cavity and, when the steady state is reached, a third run with the BHM to calculate the temperature evolution in each FDTD cell. After each iteration the dielectric and thermal properties of object's media are updated taking into account the process time and the temperature-dependent variations. This process is iteratively repeated according to a final temperature or heating time targets. In QW-3D, the average temperature of each material is calculated as a sum of products of temperature in each FDTD cell and its volume, divided by the overall volume of the FDTD cells.

Fig. 2b shows the simulation of the time evolution of the average temperature of the sample for a microwave power P_d = 10 W, heating time steps of 5 s and different interface boundary conditions between sample and tube. Parameters of simulation are given in Table 1. No wall losses are considered in the QW-3D model.

The first scenario examines the sample in the microwave cavity without the tube container. The simulated temperature of the body using QW-3D shows an asymptotic increase reaching a final equilibrium depending on the thermal heat losses in the microwave cavity. All the microwave power is absorbed in the sample, and the thermal losses affect to the whole material surface. The same mass and area of the rod-shaped material with thermal parameters of Table 1, has been simulated with the 0DM and represented for comparison. As the figure shows, the estimation of the body's average temperature with the 0DM reproduces very well the QW-3D simulation, despite not considering thermal diffusion inside the material.

Next simulated scenarios include the quartz sample holder. In these configurations, microwaves are only absorbed in the sample because dielectric losses of quartz are negligible. However, the container experiments heat due to the thermal contact at the interface material-

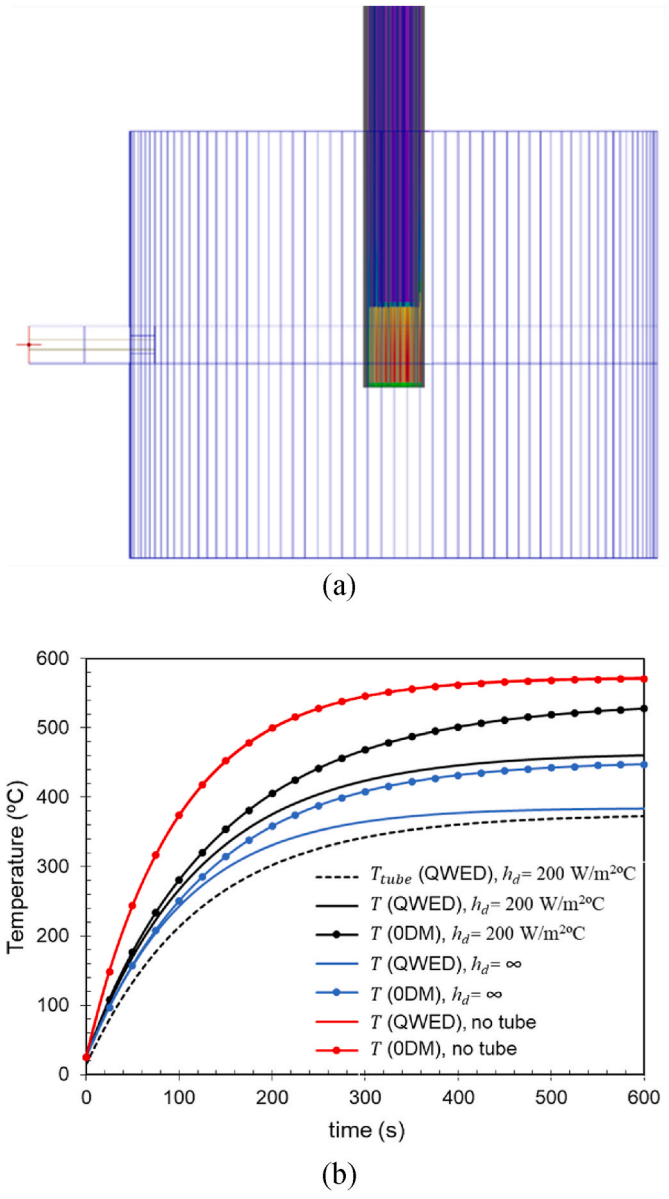

Fig. 2. (a) QW3D model of the microwave calorimeter, standard colormap, 25 °C (blue), 150 °C (red). (b) Time-evolution of average temperature of the material in the cavity as a function of h_d simulated with the QW-3D and 0DM thermal models.

Table 1
Media Parameters employed in the simulations.

Media properties	Sample (25 °C)	Sample (600 °C)	Quartz (25 °C)	Quartz (600 °C)
ε' [26,41]	5.990	5.990	3.780	3.780
ε'' [26,41]	$35{\cdot}10^{-4}$	$35{\cdot}10^{-4}$	$1{\cdot}10^{-4}$	$1{\cdot}10^{-4}$
ρ (g/cm^3) [26, 41]	2.520	2.520	2.200	2.200
c_p (J/g°C) [41, 42]	0.768	1.253	0.658	1.296
k (W/m°C) [41, 42]	1.460	1.460	1.960	1.960
h_{ext} (W/m$^{2\circ}$C) [31]	–	–	13.200	31.900
h_d (W/m$^{2\circ}$C)	200	200	–	–

quartz and extends the convective area associated to the thermal losses. For example, for a thermal resistance $h_d = \infty$, the inner surface of the quartz holder follows the temperature of the outer face of the sample (Dirichlet condition). The QW-3D simulation of the average temperature of the body exhibits a similar asymptotic increase with heating time but with lower final temperature compared to the previous simulation without tube (~380 °C instead of 580 °C), which suggests that the presence of the tube increases the thermal losses. By estimating the mass and area of the rod-shaped material and the quartz cylinder surrounding the sample, as indicated in Eqs (8) and (9), temperature results of the 0DM fit quite well with the QW-3D simulations at low temperatures (<100 °C) but overestimates the final temperatures provided by QW-3D simulator. If the thermal resistance is fixed to $h_d = 200$ W/m$^{2\circ}$C, the QW-3D simulated temperature evolves to a final temperature higher than the simulation with $h_d = \infty$ since the tube acts as small insulation jacket, but again below the final temperature reached without the tube. As in the previous case, results provided by the 0DM overestimate the final steady temperature.

The average temperature of the tube, also represented in Fig. 2b, follows an approximate ratio of 1:1.25 respect to the bulk temperature of the body. Precisely, the value of $h_d = 200$ W/m$^{2\circ}$C has been selected in the QW-3D to provide a bulk material and surface container temperature ratio comparable to the ratio achieved after temperature calibration of the IR pyrometer by the abovementioned procedure [29].

The fact that 0DM overestimates the temperature evolution is attributed to the effective area A_{ext} and mass of the quartz container might be different in both simulation approaches. In previous simulations, QW-3D includes the whole tube of Fig. 1 and the thermal diffusion along its height whereas 0DM only considers the quartz cylinder surrounding the sample.

Fig. 3a shows the simulated temperature distribution in the sample and tube for $h_d = 200$ W/m^{2}C and heating time $t = 70$ s. The figure displays a good uniform temperature distribution in the material and how the heat exchange with the tube and the thermal conductivity of quartz causes a progressive decay of temperature along the length of the tube from the sample's position to the other extreme of the tube. The effect of thermal conductivity of this temperature distribution for different heating steps is represented in Fig. 3b, which has been normalized respect to the maximum temperature in the tube. The observation of this temperature profile indicates that the mass m_t and the convective area A_{ext} of the heated tube, defined in Eq. (9), is higher that the fragment of tube surrounding the sample, but it does not reach the complete tube height. The heated volume of the tube and its evolution with temperature can be calculated by integrating the area constituted by the normalized temperature profile of Fig. 3b and related with an equivalent length l_{eq} assuming a capillary tube cross-section, as represented in Fig. 4a.

For example, Fig. 4b illustrates when l_{eq} is introduced in the 0DM, the new values of mass and area lead to the average temperature distribution of the material fit very well the simulation provided by QW-3D. However, by assuming the complete length of the quartz inside the cavity ($l_t = 75$ mm), the 0DM underestimates the temperature due to the excessive mass and area of the tube, otherwise if only the tube section around the sample is assumed ($l_t = 15$ mm), there is an overestimate of temperature in the sample. Therefore, even though quartz is not heated by microwave power, h_d drives the heat exchange between sample and tube and has a direct influence in the net absorbed power and its relationship with the temperature increase in both materials.

Extensive QW-3D simulations have been carried out for materials with a dielectric constant between 1 and 100 and a loss factor between 10^{-4} and 10. In this range and considering the sample size of Fig. 1, the homogeneity of the heating has been proven enough to provide the specific volume, mass, and convective area of the sample container necessary to evaluate the thermal losses in the microwave cavity making 0DM formulation suitable for modelling the microwave calorimeter.

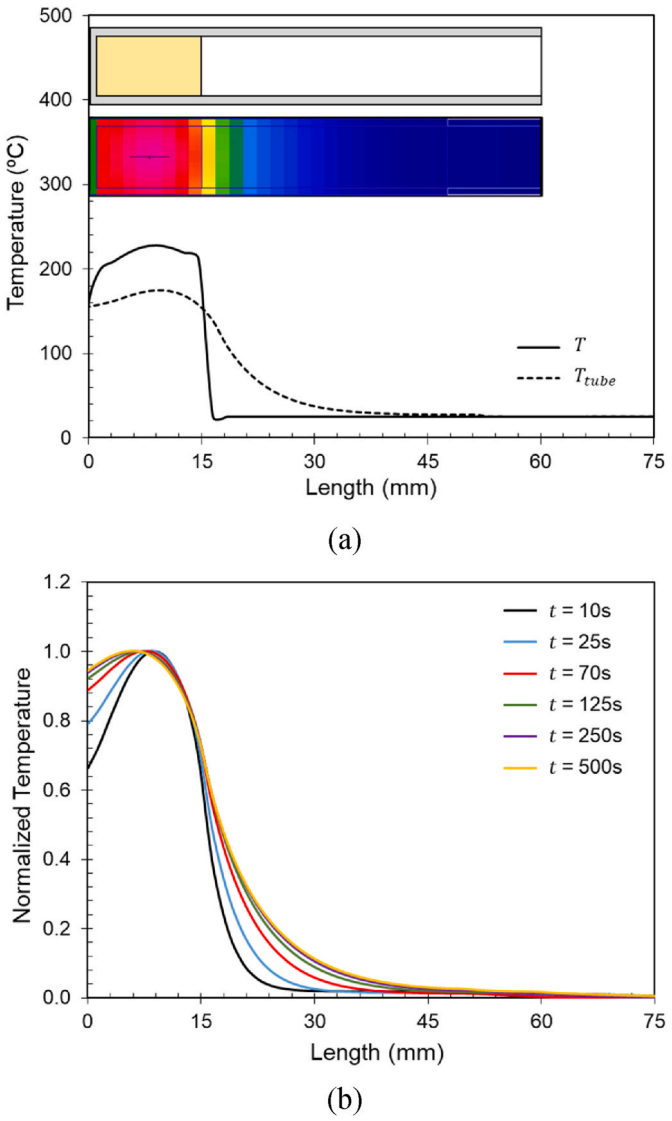

Fig. 3. (a) QW-3D simulated temperature distribution in the sample and tube for heating time t = 70s, standard colormap, 25 °C (blue), 175 °C (pink). (b) Normalized temperature distribution along the tube for different heating steps.

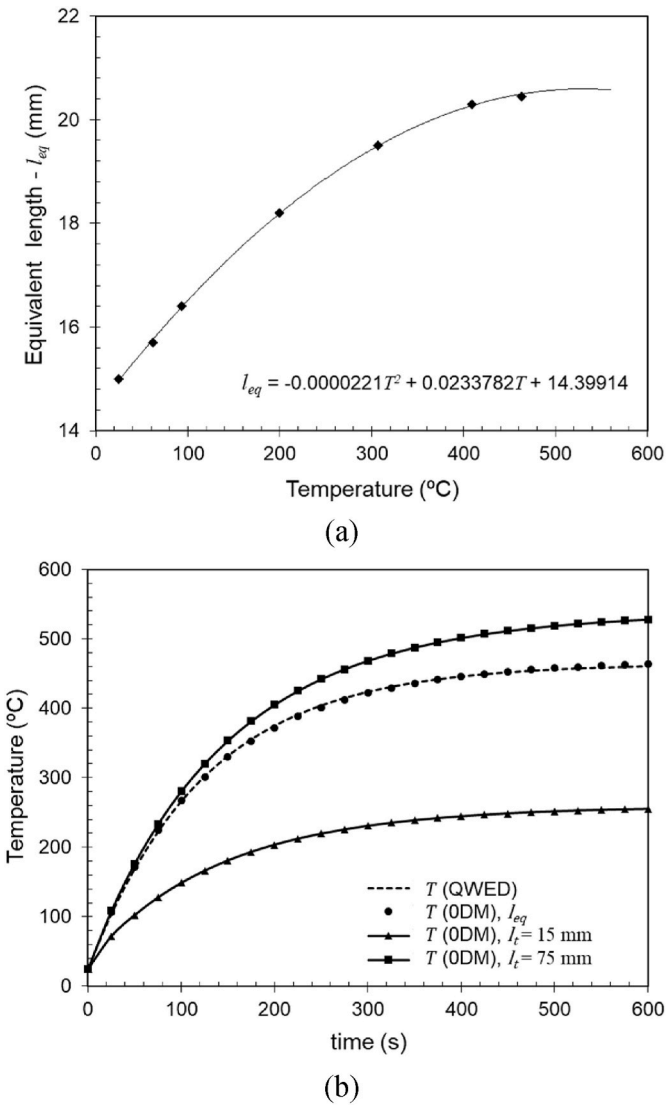

Fig. 4. (a) Equivalent length (l_{eq}) of the heated tube versus the average temperature of the sample. (b) Temperature of the sample as a function of time considering different length of the quartz tube.

3.3. Thermal losses

An extended procedure to evaluate the heat losses h_t consist of measuring the natural cooling of the material from high temperature when heat is exchanged with the surrounding fluid to reach room temperature. Assuming that the heat transfer is slow enough to maintain the temperature uniform within the object, Newton's law of cooling normally predicts an exponential curve to describe the rate of heat loss (dT/dt) from a body [43]. However, this procedure implies the knowledge of the heat capacity C of a reference sample which may not be easily available.

An alternative proposed here is based on the application of several cycles of microwave power to the microwave cavity loaded with the material to find the equilibrium temperature of the sample with the environment. Under this steady-state conditions, the amount of microwave power dissipated in dielectric heating is the same as the energy lost for convection and radiation. For each microwave power, the equilibrium temperature is reached when the heating rate is zero, then:

$$\frac{dT}{dt} = 0 \rightarrow P_d = h_t A (T - T_0) \tag{15}$$

From Eq. (15), by representing the microwave power settings P_d as a function of the bulk temperature, the factor h_tA can be calculated directly as the slope of this relation. In fact, it is not strictly necessary to separate the convection coefficient and the area since Eq. (10) requires the combined term h_tA to determine the net power absorbed by the sample. This term depends on the convection and radiation surface geometry to a greater extent and not so much on one specific material. In many practical cases, the relation of P_d with the temperature can be approximated by a second-degree polynomial function, thus h_tA normally shows a linear variation with temperature [44].

3.4. Dielectric measurements

Dielectric properties of the samples are determined from dynamic measurements of the resonance parameters of the testing mode in the microwave cavity as a function of temperature by the CPM [22,45]. In the CPM, the dielectric properties of the sample are calculated by measuring the relative changes of the unloaded resonant frequency and the quality factor of the empty cavity (f_{u0}, Q_{u0}) and cavity with the sample (f_u, Q_u), according to the relationships.

$$\varepsilon' = 1 + \frac{\Delta f}{f}\frac{1}{\kappa\eta} \tag{16}$$

$$\varepsilon'' = \Delta\left(\frac{1}{2Q}\right)\frac{1}{2\kappa\eta} \tag{17}$$

with

$$\frac{\Delta f}{f} = \frac{f_u - f_{u0}}{f_u} \tag{18}$$

$$\Delta\left(\frac{1}{2Q}\right) = \frac{f_{u0}}{f_u}\cdot\frac{1}{2}\cdot\left(\frac{1}{Q_u} - \frac{1}{Q_{u0}}\right) \tag{19}$$

where κ and η refer to the filling factors of the dielectric sample in the cavity which are directly related to the sample and cavity geometries and specific E-field configuration [46].

In the dual-model cylindrical cavity of Fig. 1a, the TM_{010} mode was designed for dielectric measurements around 2.1 GHz, whereas the TE_{111} mode was selected for microwave heating in the proximity of 2.45 GHz. Then the above equations initially refer to the testing mode of the cavity. Nevertheless, since both modes have a maximum of E-field in the area where the sample is located, both resonance modes could be used for dielectric measurements from Eqs (16) and (17) by calibrating the filling factors for each specific configuration with reference samples of known permittivity [47–50]. Once κ, η are established for both modes, and assuming that the variation of dielectric properties of materials from 2.1 GHz to 2.4 GHz is negligible, the dielectric properties of materials calculated from resonant measurements in the testing TM_{010} mode could be used to estimate the resonant frequencies and Q-factors variations of these materials into the cavity in the heating TE_{111} mode and vice versa.

3.5. Microwave losses in metal walls

The microwave power P_{mw} transmitted to the cavity from the heating source, after removing the reflected power is dissipated in the dielectric materials P_d and in the cavity metallic walls P_{walls}.

$$P_{mw} = P_d + P_{walls} \tag{20}$$

The dissipated power in the cavity is directly related to the microwave concept of the Q-factor resonance parameter [51]. The unloaded Q-factor of a finite-conductivity resonant microwave cavity containing a dielectric material, Q_u, is defined as,

$$Q_u = \frac{\omega_u W}{P_{mw}} = \frac{\omega_u W}{P_d + P_{walls}} \tag{21}$$

where ω_u stands for the resonant frequency and W is the stored energy. Then, the Q-factors associated to the losses in the dielectric material and cavity walls Q_m and Q_{u0} are related as [52]:

$$\frac{1}{Q_u} = \frac{1}{Q_m} + \frac{1}{Q_{u0}} \tag{22}$$

Therefore, it is followed:

$$\frac{P_{walls}}{P_d} = \frac{Q_m}{Q_{u0}} \tag{23}$$

From (21) and (23), the dissipated power in the cavity walls can then be expressed as

$$P_{walls} = P_{mw}\frac{Q_u}{Q_{u0}} \tag{24}$$

and the dissipated power in the dielectric material

$$P_d = P_{mw}\left(1 - \frac{Q_u}{Q_{u0}}\right) \tag{25}$$

Then, the continuous determination of dielectric properties of the dielectric material of the testing mode of the cavity during the microwave heating are used to calculate the resonance parameters (Q_u) of the heating mode with Eqs. (17) and (19) which in turn are employed to quantify the temperature dependent dissipated power in the cavity walls according to Eq. (24).

A Sankey diagram of the power distribution of the complete microwave heating process is illustrated in Fig. 5. The output of the microwave amplifier launches the microwaves (MW inlet power) into the cavity via a directional coupler. The directional coupler decouples the reflected signal (Reflected power) from the cavity to a second channel, allowing the signal to be monitored and removed from the contribution that it is introduced in the microwave cavity (Absorbed power). The dielectric properties of the material determine the amount of microwave power dissipated in the sample (Dielectric Power) and in the cavity metallic walls (Wall losses). A fraction of the dielectric power heats the sample (Net Power) and the rest is lost as conduction, convection and radiation (Thermal losses). These thermal losses are quantitively measured and together with the wall losses settle the losses (Total losses) inside the cavity.

4. Measurements, experimental results & discussion

Extensive measurements have been carried out to test the performance of the method described in previous sections. Macor, a glass-ceramic developed by Corning Inc. was selected as Material Under Test (MUT) since it remains continuously stable to more than 400 °C and because the possibilities to machine the sample according to the geometry of Fig. 1.

4.1. Experimental procedure

Several samples of Macor were machined in rods of 15 mm height and approximately 9.8 mm diameter (~2.85 g) to fit inside the quartz tubes containers. Special care should be taken when machining the sample to fit very precisely the inner diameter of the quartz tube and avoid any air gaps that could have an influence in the thermal contact between the Macor and quartz, according to the thermal model explained in previous section. The sample inside the tube was positioned at the center of the cavity through the hole in the upper wall.

Unlike conventional DSC with very limited experimental heating operation modes, the microwave calorimeter is capable of working with several regimes either constant or variable heating rates. In these experiments, two heating strategies were implemented, a quasi-constant microwave power (variable heating rate) and constant heating rate. In both strategies, the settings of the microwave heating source were automatically adjusted by the PID control procedure to achieve the desirable level of heating rate in the dielectric sample [26].

Fig. 6 shows the measurement of the time evolution of the Macor sample temperature processed in the microwave cavity for both heating

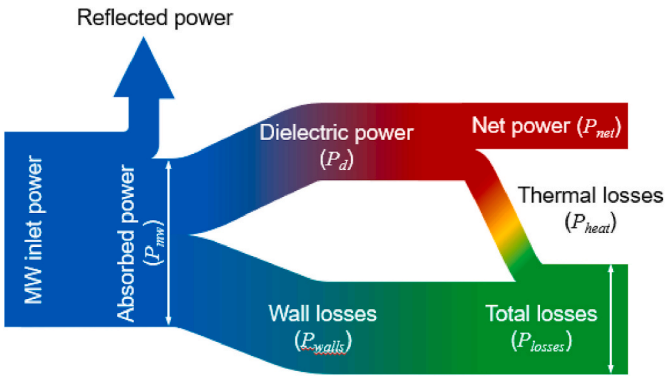

Fig. 5. Sankey diagram of the power distribution in the microwave heating process.

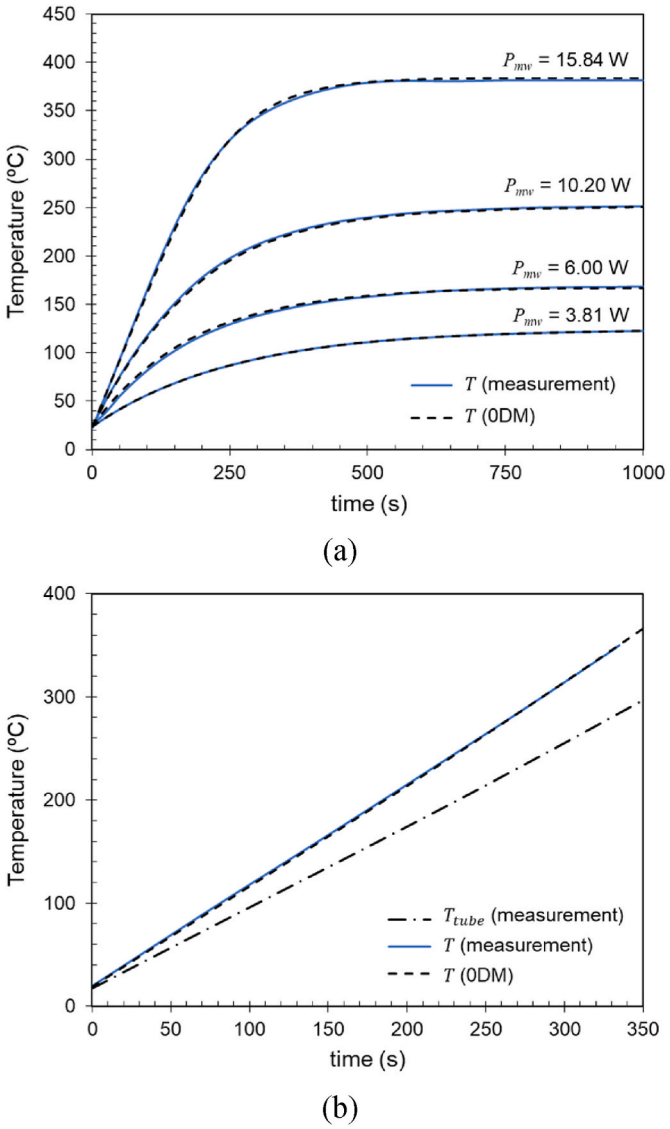

Fig. 6. Measurement of time evolution of the bulk temperature of Macor in the microwave cavity. Results of 0DM also represented in dashed lines. (a) quasi-constant microwave power cycles (variable heating rate) (b) Linear heating rate (1 °C/s.).

strategies. Results of 0DM computed after power balance calculations are also presented in dashed lines and will be explained at the end of this section.

Fig. 6b also includes the surface temperature measured by the IR pyrometer where it is possible to appreciate a ratio of 1:1.25 respect to the bulk temperature, according to the calibration procedure reported in Ref. [29]. In all cases, the dynamic measurement of the resonance parameters in the testing mode of the cavity was used to determine the dielectric properties of the Macor sample as a function of the temperature, and they are represented in Fig. 7.

4.2. Measurement of the microwave losses in metal walls

The measured dielectric properties of the Macor sample, as explained in previous Section 2, were used to estimate the unloaded Q-factor Q_u of the heating mode (TE_{111}) of the microwave cavity with the CPM Eqs. (16) and (17), and then determine the fraction of microwave power dissipated in the metallic walls P_{walls}. Fig. 8 displays the different power contributions inside the cavity as a function of the bulk temperature of the sample for both heating strategies. These calculations are of utmost

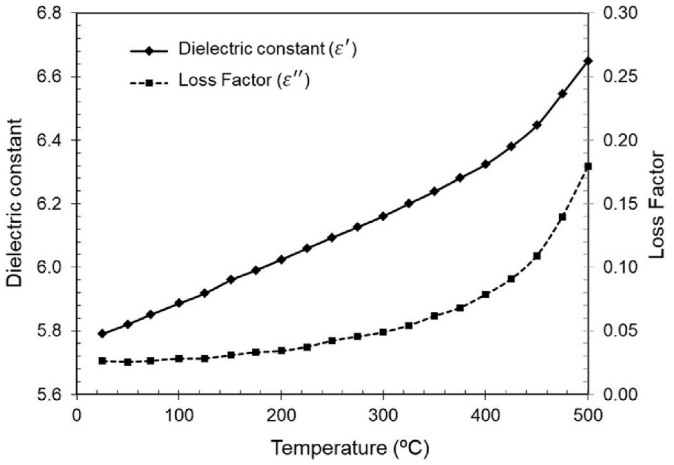

Fig. 7. Dielectric properties of Macor as a function of temperature.

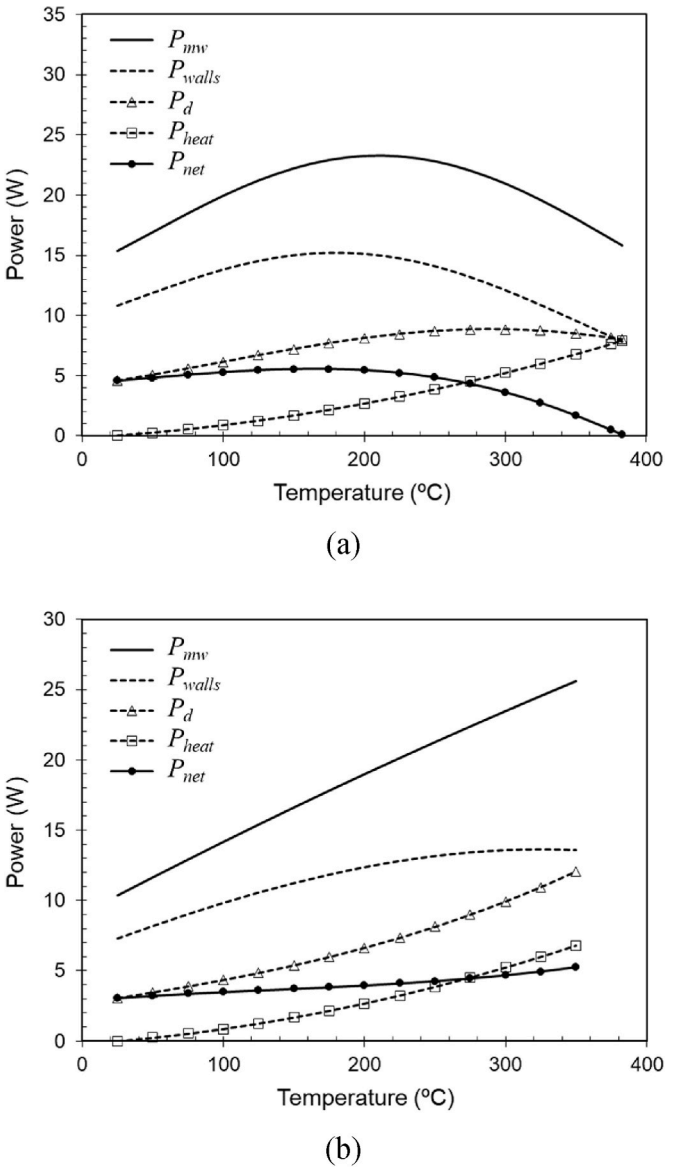

Fig. 8. Distribution of microwave power and thermal losses inside the microwave cavity for different heating strategies. (a) Variable heating rate. (b) Constant heating rate.

importance to achieve quantitative measurements in the microwave calorimeter. For example, at room temperature, for an approximate P_{mw} = 15.3 W, the microwave power dissipated on the metallic walls is about P_{walls} = 10.8 W which represents more than 70% of the power inside the cavity. As the dielectric properties of Macor increment with temperature, the sample increases the microwave absorption and the fraction of power dissipated on the walls at 350 °C falls to 7.8 W (50%).

4.3. Measurement of the thermal losses

After removing the dissipation in the walls, the rest of the microwave power P_d is absorbed by the materials increasing their temperature and exchanging thermal energy with the surroundings. Measurements of Fig. 6a show that during the quasi-constant microwave power cycles, and in the absence of phase transformations accompanied with changes in the internal energy of the sample, the temperature of Macor increases monotonically to compensate the heat losses until reaching an equilibrium. By representing these equilibrium temperatures and the dielectric power values P_d, the slope of this representation directly provides the factor h_tA, according to Eq. (15). As shown in Fig. 9, the variation of dielectric power can be approximated by a second-degree polynomial representation and consequently the term h_tA follows a linear variation with temperature. This experimental result confirms the assumption of the heat transfer model of Eq. (6) that combines the Newton and the Stefan-Boltzmann law in a unique h_t coefficient for this range of temperatures.

Once the thermal losses have been determined, we can calculate the balance of power in the cavity quantifying all the terms described by Eqs. (1)–(3). For the first heating strategy with a quasi-constant microwave power, Fig. 8a shows that the equilibrium temperature is achieved when the net power is null. In the constant heating rate strategy, the net power slightly increases with the temperature, being the dielectric power always higher than the heat losses of the system. For example, in this second case, at 350 °C, the figure shows that from the total microwave power in the cavity P_{mw} = 25.6 W, the amount of microwave power dissipated in the walls is P_{walls} = 13.5 W and the thermal losses are P_{heat} = 6.7 W which results in a net power P_{net} = 5.2 W.

4.4. Measurement of the heat capacity

Heat capacity C of the tube and sample as a function of temperature are estimated as the ratio between the net power P_{net} and the heating rate dT/dt, according to Eq. (11). Fig. 10a shows the heating rate of both strategies, calculated from the power curves of Fig. 6. The constant heating rate depicts an approximate value of 1 °C/s while the variable heating rate decreases from around 1.4 °C/s to 0 °C/s.

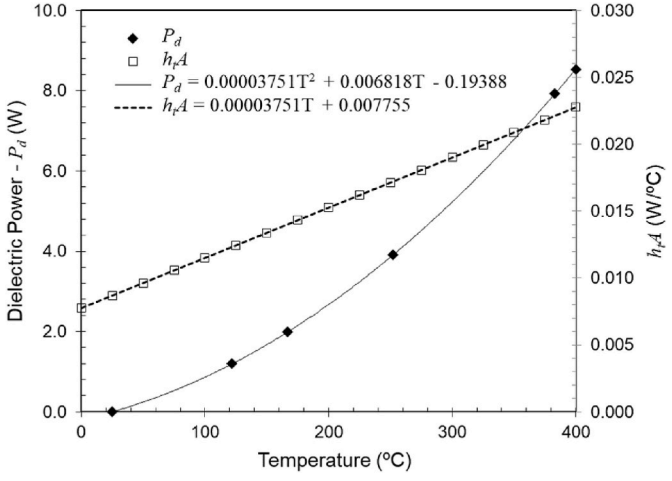

Fig. 9. Dielectric power and convection coefficient as a function of the bulk temperature.

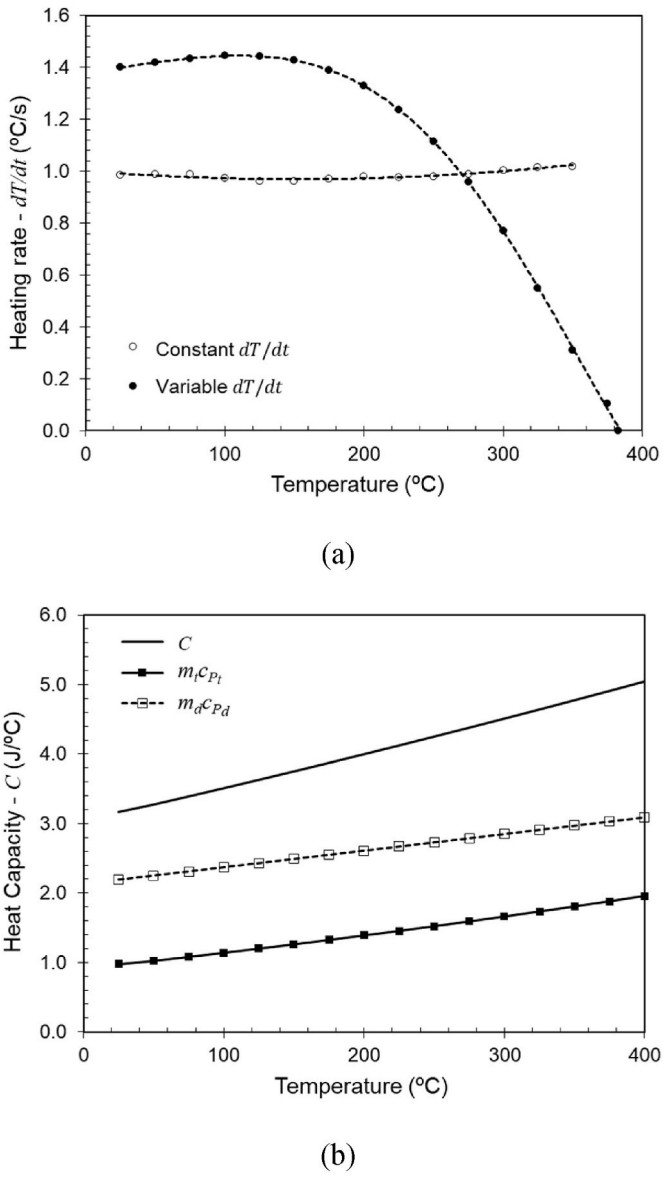

Fig. 10. (a) Heating rate versus bulk temperature of the sample for different heating strategies. (b) Heat capacity C of combined, quartz and Macor as a function of temperature versus temperature.

Heat capacity of combined and specific for each material are represented in Fig. 10b and the specific heat of Macor c_{P_d}, dividing heat capacity by the mass of the sample (2.85 g), in Fig. 11. No changes of mass were considered during the heating process. To achieve these results, we assumed that the temperature of quartz heated during the experiments follows the profile simulated in Section 3 and therefore the mass of quartz was determined from the l_{eq} of Fig. 4a.

The specific heat of Macor has also been measured by a conventional DSC (NETZSCH STA 449 F3 Jupiter) with a heating rate of 0.17 °C/s in air atmosphere, and it is represented in Fig. 11 for comparison. From the figure, very good agreement between both methods is observed highlighting the performance of the microwave method independently of the strategy employed to heat the sample.

To ensure the validity of the whole process, the measured thermal parameters (h_tA and C) and the microwave power dissipated in the material P_d of Fig. 8 were introduced in the 0DM of Eq. (14) to compute the temperature evolution of the sample and they are represented in Fig. 6 for comparison. Again, very good agreement is observed with the

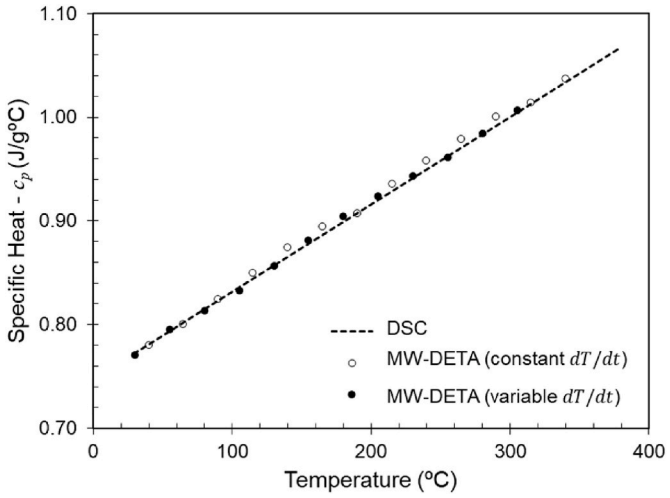

Fig. 11. Specific heat of Macor measured with MW-DETA versus conventional DSC.

measurement results despite 0DM does not consider temperature gradients inside the material.

5. Conclusions

A fast method for determining dielectric and thermal properties of a sample of material as a function of temperature by microwave heating has been developed (MW-DETA). Unlike previous microwave methods with differential results, the method reported here provides for the first time quantitative measurements of the thermal parameters of materials, as the specific heat, which could be of great interest, specially to evaluate the energy requirements of microwave heating processes.

The method is based on a dual-mode cylindrical microwave cavity where microwave heating and simultaneous monitoring of dielectric properties of materials are feasible. The measured dielectric properties of the sample with temperature and the precise numerical modelling of the thermal process provided the necessary information to quantify the thermal and microwave losses in the cavity and therefore the precise fraction of power delivered to the sample.

In a similar manner to previous microwave approaches, the MW-DETA is capable to operate automatically in a wide range of heating modes, either constant or variable heating rates, by adjusting the settings of the microwave heating source by a PID procedure.

The functionality of the microwave calorimeter has been demonstrated by heating and measuring a ceramic sample of Macor up to 400 °C. The performance of the method in the measurements has been validated by comparison with conventional DSC measurements.

The design of the calorimetric measurements described in previous sections is restricted to homogenous samples placed inside quartz vials with specific dimensions to ensure an intense and homogeneous heating inside the microwave cavity. With this configuration, the application of microwaves ensures a fast heating to extract thermal parameters of materials. Heterogeneous materials, as food products, could experience differential internal heating due to the selectivity effect of microwave heating and the formation of local high-temperature points that might limit the speed of the microwave calorimeter for these materials.

Credit author statement

Juan R. Sánchez: Methodology, Investigation, Validation, Writing – original draft. **José D. Guitérrez-Cano**: Investigation, Validation. **Pedro J. Plaza-González**: Software, Investigation. **Felipe L. Penaranda-Foix**: Software, Visualization. **José M. Catalá-Civera**: Conceptualization, Writing – review & editing, Supervision.

Declaration of competing interest

The authors declare that they have no known competing financial interests or personal relationships that could have appeared to influence the work reported in this paper.

Data availability

No data was used for the research described in the article.

Acknowledgements

This research project has received funding from the Ministerio de Universidades by the European Union– NextGenerationEU programme under the grant Margarita Salas (MS/2).

Funding for open access charge: CRUE-Universitat Politècnica de València.

References

[1] Serra JM, et al. Hydrogen production via microwave-induced water splitting at low temperature. Nat Energy 2020;5(11):910–9. https://doi.org/10.1038/s41560-020-00720-6.
[2] Wang W, et al. Quantitative measurement of energy utilization efficiency and study of influence factors in typical microwave heating process. Energy 2015;87:678–85. https://doi.org/10.1016/j.energy.2015.05.036. Jul.
[3] Kasap S, Málek J, Svoboda R. Thermal properties and thermal analysis: fundamentals, experimental techniques and applications. Springer; 2017. https://doi.org/10.1007/978-3-319-48933-9_19.
[4] Gallagher PK. Handbook of thermal analysis and calorimetry. first ed. Amsterdam: Elseiver; 2008.
[5] Wunderlich B. Thermal analysis of polymeric materials. first ed. Knoxville, TN: Springer; 2005. https://doi.org/10.1007/b137476.
[6] Prime RB, Bair HE, Vyazovkin S, Gallagher PK, Riga A. Thermogravimetric analysis (TGA). Thermal analysis of polymers: Fundamentals and applications 2009: 241–317.
[7] Kodre K, Attarde S, Yendhe P, Patil R, Barge V. Differential scanning calorimetry: a review. J Pharm Anal 2014;3(3):11–22.
[8] Brown ME. Differential thermal analysis (DTA) and differential scanning calorimetry (DSC). In: Introduction to thermal analysis: techniques and applications. Dordrecht: Springer Netherlands; 1988. p. 23–49. https://doi.org/10.1007/978-94-009-1219-9_4.
[9] Richardson MJ. The application of differential scanning calorimetry to the measurement of specific heat. In: Maglić KD, Cezairliyan A, Peletsky VE, editors. Compendium of thermophysical property measurement methods: volume 2 recommended measurement techniques and practices. Boston, MA: Springer US; 1992. p. 519–45. https://doi.org/10.1007/978-1-4615-3286-6_18.
[10] Ehrenstein GW, Riedel G, Trawiel P. Thermal analysis of plastics. first ed. Cincinnati: Hanser; 2004 [Online]. Available: www.hanser-elibrary.com.
[11] Leturcq P, Dorkel J-M, Napieralski A, Lachiver E. A new approach to thermal analysis of power devices. IEEE Trans Electron Dev 1987;34(5):1147–56. https://doi.org/10.1109/T-ED.1987.23057.
[12] Karathanasis AD. Thermal analysis of soil minerals. In: Methods of soil analysis Part 5-mineralogical methods. John Wiley & Sons, Ltd; 2008. p. 117–60. https://doi.org/10.2136/sssabookser5.5.c5.
[13] st S, Warne J. Differential thermal analysis of coal minerals. In: KARR C, editor. Analytical methods for coal and coal products. Academic Press; 1979. https://doi.org/10.1016/B978-0-12-399903-0.50021-0.
[14] Parkes GMB, Barnes PA, Charsley EL, Bond G. Microwave thermal analysis - a new approach to the study of the thermal and dielectric properties of materials. J Therm Anal Calorim 1999;56:723–31.
[15] Zhuravlev E, Schick C. Fast scanning power compensated differential scanning nano-calorimeter: 1. The device. Thermochim Acta 2010;505(1–2):1–13. https://doi.org/10.1016/j.tca.2010.03.019. Jun.
[16] Quick CR, Schawe JEK, Uggowitzer PJ, Pogatscher S. Measurement of specific heat capacity via fast scanning calorimetry-Accuracy and loss corrections. Thermochim Acta 2019;677:12–20. https://doi.org/10.1016/j.tca.2019.03.021. Jul.
[17] Karmazsin E, Barhoumi R, Satre P. Thermal analysis with microwaves: temperature and power control. J Therm Anal 1984;29:1269–77. May.
[18] Karmazsin E, Barhoumi R, Satre P, Galliard F. Use of microwaves in thermal analysis. J Therm Anal 1985;30:43–7.
[19] Dudley GB, Richert R, Stiegman AE. On the existence of and mechanism for microwave-specific reaction rate enhancement. Chem Sci 2015;6(4):2144–52. https://doi.org/10.1039/c4sc03372h. Apr.
[20] Garcia-Baños B, Catalá-Civera JM, Peñaranda-Foix FL, Plaza-González P, Llorens-Vallés G. In situ monitoring of microwave processing of materials at high temperatures through dielectric properties measurement. Materials 2016;9(5). https://doi.org/10.3390/ma9050349.
[21] Yan B, Jiao L, Li J, Zhu X, Ahmed S, Chen G. Investigation on microwave torrefaction: parametric influence, TG-MS-FTIR analysis, and gasification

performance. Energy 2021;220. https://doi.org/10.1016/j.energy.2021.119794. Apr.
[22] Jafari H, Kalantari D, Azadbakht M. Energy consumption and qualitative evaluation of a continuous band microwave dryer for rice paddy drying. Energy Jan. 2018;142:647–54. https://doi.org/10.1016/j.energy.2017.10.065.
[23] Parkes GMB, Barnes PA, Bond G, Charsley EL. Qualitative and quantitative aspects of microwave thermal analysis. Thermochim Acta 2000;356(1–2):85–96. https://doi.org/10.1016/S0040-6031(00)00458-5.
[24] Parkes GMB, Bond G, Barnes PA, Charsley EL. Development of a new instrument for performing microwave thermal analysis. Rev Sci Instrum 2000;71(1):168–75. https://doi.org/10.1063/1.1150179.
[25] Nesbitt A, et al. Development of a microwave calorimeter for simultaneous thermal analysis, infrared spectroscopy and dielectric measurements. Meas Sci Technol 2004;15(11):2313–24. https://doi.org/10.1088/0957-0233/15/11/018.
[26] Catalá-Civera JM, Canós AJ, Plaza-González P, Gutiérrez JD, García-Baños B, Peñaranda-Foix FL. Dynamic measurement of dielectric properties of materials at high temperature during microwave heating in a dual mode cylindrical cavity. IEEE Trans Microw Theor Tech 2015;63(9):2905–14. https://doi.org/10.1109/TMTT.2015.2453263. Sep.
[27] Shen X, Li H, Zhao Z, Li X, Liu K, Gao X. Imaging of liquid temperature distribution during microwave heating via thermochromic metal organic frameworks. Int J Heat Mass Tran 2022;189. https://doi.org/10.1016/j.ijheatmasstransfer.2022.122667. Jun.
[28] Zhao Z, et al. Watching microwave-induced microscopic hot spots via the thermosensitive fluorescence of europium/terbium mixed-metal organic complexes. Angew Chem Int Ed 2022;61(6). https://doi.org/10.1002/anie.202114340. Feb.
[29] García-Baños B, Reinosa JJ, Peñaranda-Foix FL, Fernández JF, Catalá-Civera JM. Temperature assessment of microwave-enhanced heating processes. Sci Rep 2019;9(1):10809. https://doi.org/10.1038/s41598-019-47296-0.
[30] Metaxas AC, (Roger J) Meredith RJ. Industrial microwave heating. first ed. London: Peter Peregrinus; 1983.
[31] Lévesque L. Law of cooling, heat conduction and Stefan-Boltzmann radiation laws fitted to experimental data for bones irradiated by CO2 laser. Biomed Opt Express 2014;5(3):701. https://doi.org/10.1364/boe.5.000701. Mar.
[32] özışık MNecati. Heat conduction. second ed. New York: Wiley; 1993.
[33] Kakac S, Cotta C, Yaman Yener Y. Heat conduction. fifth ed. Boca Raton, FL: Taylor & Francis; 2018 [Online]. Available: http://taylorandfrancis.com.
[34] Besson U. Cooling and warming laws: an exact analytical solution. Eur J Phys 2010;31(5):1107–1121, Sep. https://doi.org/10.1088/0143-0807/31/5/013.
[35] Howell JR, Menguc MP, Siegel R. Thermal radiation heat transfer. fifth ed. Boca Raton, FL: Taylor & Francis Group; 2010.
[36] Conti R, Gallitto AA, Fiordilino E. Measurement of the convective heat-transfer coefficient. 2014. https://doi.org/10.1119/1.4862118. Jan.
[37] Sen M. Analytical heat transfer. Notre Dame: University of Notre Dame; 2017.
[38] Cooper MG, Mikic BB, Yovanovich M. Thermal contact conductance. Int J Heat Mass Tran 1969;12:279–300. https://doi.org/10.1016/0017-9310(69)90011-8. Jun.
[39] Yuan W, Yu N, Li L, Fang Y. Heat transfer analysis in multi-layered materials with interfacial thermal resistance. Compos Struct 2022;293:115728. https://doi.org/10.1016/j.compstruct.2022.115728. Aug.
[40] QUICKWAVE. Software for electromagnetic design and simulations. 2020 [Online]. Available: https://www.qwed.eu/QuickWave_2020.pdf.
[41] Nigar H, et al. Numerical analysis of microwave heating cavity: combining electromagnetic energy, heat transfer and fluid dynamics for a NaY zeolite fixed-bed. Appl Therm Eng 2019;155:226–38. https://doi.org/10.1016/j.applthermaleng.2019.03.117. Jun.
[42] Corning. MACOR ® machinable glass ceramic for industrial applications. 2022.
[43] O'Sullivan C. A simple experiment to study cooling by convection and radiation. 2006. Oct.
[44] Marín E. Linear relationships in heat transfer. Am. J. Phys. Educ 2009;3(2):243–5 [Online]. Available: http://www.journal.lapen.org.mx.
[45] Harrington RF. Time-harmonic electromagnetic fields. New York: Wiley; 2001. https://doi.org/10.1109/9780470546710.fmatter.
[46] Khanna SK, Ehrenfreund E, Garito AF, Heeger AJ. Microwave properties of high-purity tetrathiofulvalene-tetracyanoquinodimethan (TTF-TCNQ). Phys Rev B 1974;10(6):2205–2220, Sep. https://doi.org/10.1103/PhysRevB.10.2205.
[47] Roussy G, Thiebaut J-M, Ename-Obiang F, Marchal E. Microwave broadband permittivity measurement with a multimode helical resonator for studying catalysts. 2001 [Online]. Available: www.iop.org/Journals/mt.
[48] Robinson MP, Flintoft ID, Dawson L, Clegg J, Truscott JG, Zhu X. Application of resonant cavity perturbation to in vivo segmental hydration measurement. Meas Sci Technol 2010;21(1). https://doi.org/10.1088/0957-0233/21/1/015804.
[49] Pohl V, Fricke D, Mühlbauer A. Correction procedures for the measurement of permittivities with the cavity perturbation method. J Microw Power Electromagn Energy 1995;30(1):10–26. https://doi.org/10.1080/08327823.1995.11688253. Jan.
[50] Adams F, de Jong M, Hutcheon R. Sample shape correction factors for cavity perturbation measurements. J Microw Power Electromagn Energy 1992;27(3):131–5. https://doi.org/10.1080/08327823.1992.11688181. Jan.
[51] Sheen J. Amendment of cavity perturbation technique for loss tangent measurement at microwave frequencies. In: 2006 7th international symposium on antennas. Propagation & EM Theory; 2006. p. 1–3. https://doi.org/10.1109/ISAPE.2006.353221.
[52] Bonincontro A, Cametti C. On the applicability of the cavity perturbation method to high-loss dielectrics. J Phys 1977;10(12):1232–3. https://doi.org/10.1088/0022-3735/10/12/013. Dec.